Journal of Power Sources 189 (2009) 391–396

Contents lists available at ScienceDirect

Journal of Power Sources

journal homepage: www.elsevier.com/locate/jpowsour

Effect of synthetic conditions on the electrochemical properties of $LiMn_{0.4}Fe_{0.6}PO_4$/C synthesized by sol–gel technique

Jae-Kwang Kim [a], Ghanshyam S. Chauhan [a], Jou-Hyeon Ahn [a,*], Hyo-Jun Ahn [b]

[a] Department of Chemical and Biological Engineering and Engineering Research Institute, Gyeongsang National University, 900 Gajwa-dong, Jinju 660-701, Republic of Korea
[b] School of Nano and Advanced Materials Engineering and Engineering Research Institute, Gyeongsang National University, 900 Gajwa-dong, Jinju 660-701, Republic of Korea

ARTICLE INFO

Article history:
Received 28 June 2008
Received in revised form 1 August 2008
Accepted 1 August 2008
Available online 9 August 2008

Keywords:
Olivine
$LiMn_yFe_{1-y}PO_4$
Sol–gel process
Electrospinning technique
Electrochemical performance

ABSTRACT

Carbon-coated $LiMn_{0.4}Fe_{0.6}PO_4$ (LMFP) was synthesized by sol–gel technique using citric acid as foaming agent and carbon precursor. To evaluate the effect of synthetic conditions on the electrochemical properties of LMFP for use as cathode active material, the carbon-coated olivines were synthesized by a two-step thermal treatment at different temperatures. The composites were characterized by elemental analysis, XRD, SEM, TEM, Raman microprobe spectroscopy and their electrochemical properties were also studied. The composite that shows the better electrochemical performance has more porous structure, lower D/G band ratio in Raman spectra, and charge and discharge capacities of same 155 mAh g^{-1} with higher material utilization of 97% at 0.1 C-rate (0.05 mA cm^{-2}). The material exhibiting the better performance was also incorporated in a polymer electrolyte hosted in an electrospun P(VdF-HFP) membrane. The lithium polymer battery composed of $LiMn_{0.4}Fe_{0.6}PO_4$ cathode and polymer electrolyte showed a good cycling performance with the initial discharge capacity of 146 mAh g^{-1}.

1. Introduction

In recent years many research groups are engaged in developing secondary lithium batteries having positive electrode materials made up of phospho-olivines ($LiMPO_4$, where M denotes Fe, Mn, Co, Ni). The cathode materials having $LiMPO_4$ structure possess good thermal stability due to the P–O covalent bonding. Therefore, these materials are suitable for use in a number of applications ranging from cellular phones, notebook computers to hybrid electric vehicles. However, the electronic conductivity of $LiMPO_4$ is much lower in comparison with $LiCoO_2$ (10^{-3} S m^{-1}), which is currently used as cathode material. Many attempts have been made to enhance the electronic conductivity of $LiMPO_4$ by optimizing synthetic conditions. These include *in situ* carbon coating on particles and doping of metal ions that coexist with Li^+ in $LiMPO_4$. In 2001, Yamada et al. reported reversible insertion/extraction of Li^+ in lithium manganese iron phosphate ($LiMn_yFe_{1-y}PO_4$) [1,2]. The variation of y in $LiMn_yFe_{1-y}PO_4$ can be used to optimize its properties to tailor a promising candidate material, as $LiMn_yFe_{1-y}PO_4$ operates at a desirable cell voltage of 3.4–4.1 V versus Li^+/Li [1,2]. The Mn^{3+}/Mn^{2+} redox couple in the olivine framework is positioned at 4.1 V versus Li/Li^+ which is reasonably high as compared to Fe^{3+}/Fe^{2+} redox couple in $LiFePO_4$. However, there are some serious drawbacks that limit the use of Mn^{3+}/Mn^{2+} redox couple as cathode material. $LiMnPO_4$ exhibits slower kinetics [3], and its current durability and effective energy density is much smaller as compared to Li_xFePO_4 [4]. One of the important reasons for its poor electrochemical activity is a large kinetic barrier at the incompatible interface of $MnPO_4/LiMnPO_4$ [4].

The synthesis of phase-pure $LiMn_yFe_{1-y}PO_4$ is a challenging task. The manipulation of the amount of Mn in the $LiMPO_4$ composition is crucial as the material with higher Mn amount has poor cycling stability. The synthesis of $LiMn_yFe_{1-y}PO_4$ by solid state reactions has been reported [5,6]. The one- or two-step synthesis of olivines by sol–gel method has been reported at temperature ranging from 300 to 700 °C [7]. The thermal treatment at low temperature and above 600 °C creates Fe_2P that improves its electronic conductivity [8]. To the contrary, materials with large pores are obtained when synthesized under 500 °C by employing sol–gel technique [9]. An *in situ* coating of carbon over the active material particles is achieved by adding citric acid as the carbon precursor [10]. The carbon coating helps to retard undesirable particle

* Corresponding author. Tel.: +82 55 751 5388; fax: +82 55 753 1806.
E-mail address: jhahn@gnu.ac.kr (J.-H. Ahn).

0378-7753/$ – see front matter © 2008 Elsevier B.V. All rights reserved.
doi:10.1016/j.jpowsour.2008.08.001

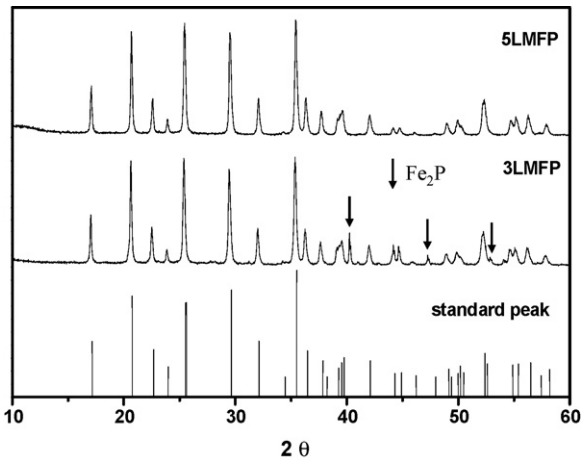

Fig. 1. XRD spectra of 3LMFP and 5LMFP in comparison to standard *Pnma* orthorhombic $LiFePO_4$.

growth during the thermal treatment, and also improves electrical conductivity of the active material [11]. The partial substitution of Mn^{2+} and carbon coating over the particle surface can significantly enhance the electrochemical performance of the olivine cathode materials [12].

In the present work, LMFP was synthesized in the presence of carbon precursor by sol–gel method, and then it was subjected to heat treatment in two steps at two different temperatures. The structural, morphological and electrochemical properties of the carbon-coated LMFP synthesized at different temperatures are compared. The carbon coated LMFP that affords the better results was applied with electrospun P(VdF-HFP) membrane based polymer electrolyte (PE). The electrospinning technique is an easy and versatile method to prepare nano-fibrous polymer membranes [13–15]. The PEs prepared by electrospinning can attain high ionic conductivity at room temperature because the membranes prepared by electrospinning have large surface area and fully interconnected pore structures. The electrospun P(VdF-HFP) microfibrous membrane based PE was prepared for conducting a

Table 1
BET surface area, pore volume, pore size and carbon D/G integrated ratio of 3LMFP and 5LMFP

Samples	BET ($m^2\ g^{-1}$)	Pore volume ($cm^3\ g^{-1}$)	Pore size (Å)	D/G
3LMFP	47.42	0.055	46.64	2.504
5LMFP	61.41	0.088	57.16	1.635

preliminary evaluation of electrochemical performance of LMFP cathodes in lithium polymer battery (LPB) at room temperature [15–17]. To the best of our knowledge, there is no report on the properties of $Li/LiMn_yFe_{1-y}PO_4$ cell using gel/polymer electrolytes. Even in the case of $Li/LiFePO_4$ cell, various studies have been reported at operating temperatures higher than 40 °C [18,19].

2. Experimental

2.1. Synthesis of cathode material

Li_2CO_3, $FeC_2O_4{\cdot}2H_2O$, $Mn(COOCH_3)_2{\cdot}4H_2O$ and $NH_4H_2PO_4$ (all chemicals of 99% purity from Aldrich) and citric acid (Shinyo Pure Chemicals, 99% purity) were used as the starting materials to synthesize LMFP composites. These were dissolved in deionized water at room temperature and to the resulting solution was added citric acid solution. After homogenous mixing, the sol was dried by keeping it at 75 °C for 12 h during magnetic stirring. The gel state obtained was placed in a vacuum oven and heated at 70 °C for 12 h. Two different sets of these mixtures were fired separately under nitrogen atmosphere in two steps: (i) at 300 °C for 3 h and 700 °C for 10 h (named as 3LMFP) and (ii) at 500 °C for 3 h and 700 °C for 10 h (named as 5LMFP).

2.2. Preparation of gel polymer electrolyte

The porous membrane of P(VdF-HFP) polymer was prepared by electrospinning process under conditions optimized in our laboratory [15]. A 17 wt.% solution of P(VdF-HFP) (Kynar Flex 2801) in a mixed solvent (7:3 by wt. ratio) of acetone and *N*,*N*-dimethylacetamide (HPLC grade, Aldrich) was electrospun in a

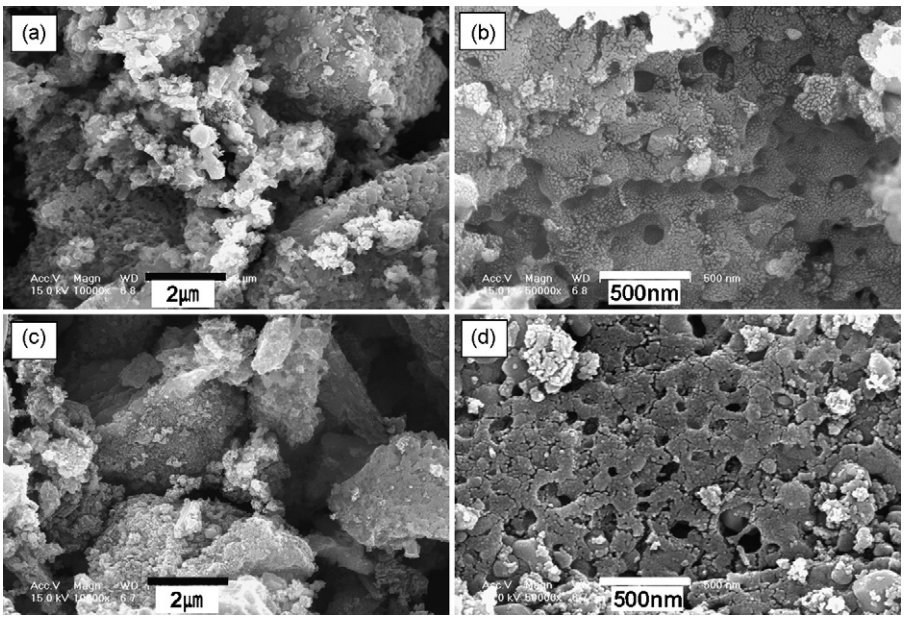

Fig. 2. SEM images of (a, b) 3LMFP and (c, d) 5LMFP.

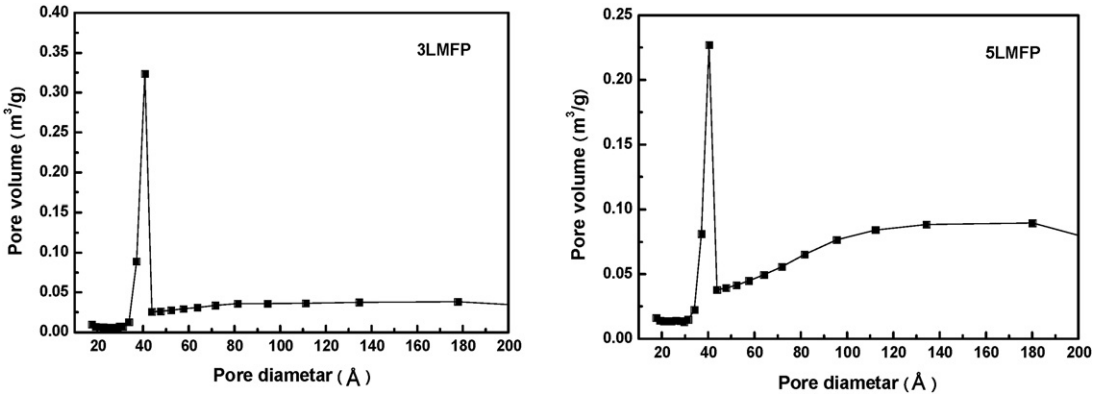

Fig. 3. Pore-size distribution for 3LMFP and 5LMFP prepared by sol–gel process.

common setup at room temperature. A homogenous and free standing membrane of ~50 μm thickness was obtained under optimized conditions. Polymer electrolyte (PE) was prepared by soaking the membrane for 10 min with a solution of 1 M $LiPF_6$ in ethylene carbonate (EC)/dimethyl carbonate (DMC) (1:1 by vol.) (battery grade, Samsung Cheil Industries Inc.) under argon atmosphere in a glove box (H_2O < 10 ppm).

2.3. Characterization of synthesized materials

The crystallographic structural characterization by X-ray powder diffraction (XRD) and Rietveld refinement was done by a SIMENS D5005 X-ray diffractometer using Cu Kα radiation (35 mA/40 kV) and a graphite monochromator. Scanning electron microscopy (SEM) imaging was done using FE-SEM (Philips XL30 S FEG). The nature and thickness of carbon coating was observed with high resolution transmission electron microscopy (HR-TEM) (JEM-3010, JEOL). The specific surface area was computed from N_2 sorption data (ASAP 2020 Analyzer) using Brunauer–Emmett–Teller (BET) method. The chemical composition of active materials was determined by inductively coupled plasma (ICP) analysis (Atomscan 25, Optima 4300DV) and carbon content by elemental analyzer (CHNS-932, LECO).

2.4. Electrochemical evaluation

To prepare the cathode, LMFP powder, super-P carbon black (Alfa) and poly(vinylidene fluoride) (PVdF, Aldrich) binder were mixed in 80:10:10 weight ratio and a viscous slurry in *N*-methylpyrrolidone (NMP) solvent was cast on aluminum foil and dried at 95 °C under vacuum for 12 h. The film was cut into circular discs of area 0.95 cm^2 and mass ~2.5 mg for use as cathodes.

The coin type Li/LMFP cell was fabricated by stacking lithium metal (300 μm thickness, Cyprus Foote Mineral Co.) anode and LMFP-based cathode with Celgard® 2200 separator film. 1 M $LiPF_6$ in EC/DMC (1:1 by vol.) was used as liquid electrolyte. In addition, the 5LMFP electrode was assembled by sandwiching the PE between lithium metal as anode. The cell assembly was performed under argon atmosphere in a glove box (H_2O < 10 ppm). The charge–discharge and cycling properties were evaluated between 2.0 and 4.4 V for liquid electrolyte, and also between 2.5 and 4.2 V for polymer electrolyte at same current density using an automatic galvanostatic charge–discharge unit (WonA Tech. Co.) at room temperature.

3. Results and discussion

The LMFP gel prepared by the sol–gel technique was converted to sponge-like porous powder in the presence of citric acid in two steps at two different temperatures. Citric acid inhibits oxidation of Fe^{2+} to Fe^{3+}, reduces any Fe^{3+} present, thus it ensures the formation of impurity free sample. The chemical composition of the samples was observed to match with the theoretical molar ratio of Li:Mn:Fe:P as 1.00:0.40:0.60:1.00 within the error range of ICP, and the two samples contain 10.0 wt.% carbon by elemental analysis.

XRD spectra of the synthesized LMFP are shown in Fig. 1. The structure is identified as orthorhombic olivine *Pnma* space group. The pattern of 5LMFP shows good correspondence with standard LMFP spectra which is also included as reference. Apart from the Fe_2P impurity phase present in the spectrum of 3LMFP, there are no significant peaks in the spectra of these samples that can be ascribed to any impurity phase. This impurity phase is associated with the synthetic mode of 3LMFP that involved a lower temperature treatment in the first step where FeP is formed which is converted to Fe_2P above 600 °C. Its presence in smaller amounts enhances electrochemical performance of LMFP [8]. SEM micro-

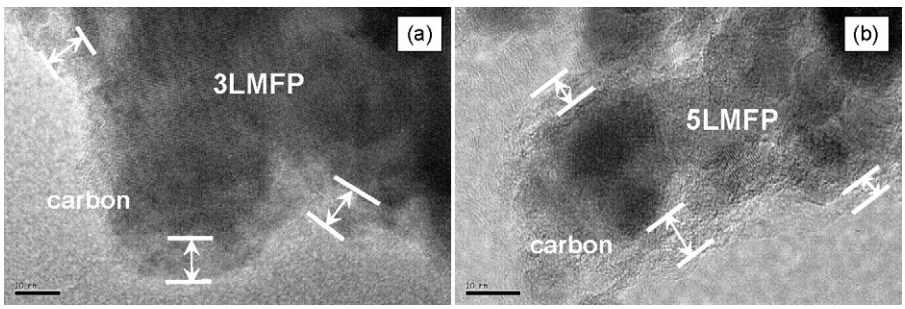

Fig. 4. TEM images of (a) 3LMFP and (b) 5LMFP.

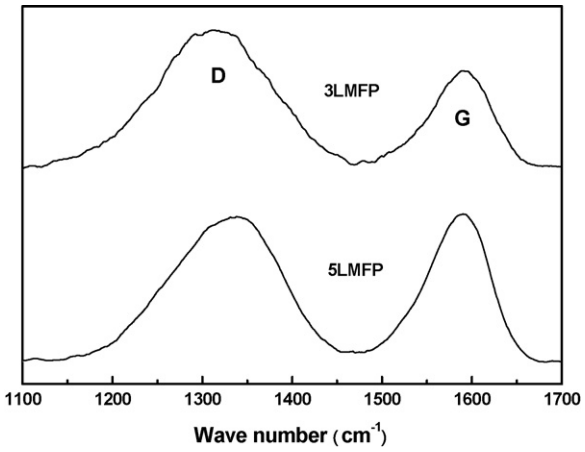

Fig. 5. Raman spectra of 3LMFP and 5LMFP.

graphs of LMFP prepared under different heating conditions are presented in Fig. 2 [(a) and (b) are of 3LMFP, while (c) and (d) are of 5LMFP]. These materials are porous and the pore walls as well as the surface of the particles are covered by carbon coating as shown in Fig. 2. The pore size, porosity and the surface morphology of LMFP are dependent on the synthetic conditions employed such as the heating temperature. The highly porous cathode materials are advantageous in lithium ion battery because the pores get filled with electrolyte that improves diffusion of Li^+. The micron-sized particles are spongy and have a homogenous morphology. Although some particle aggregation does take place to yield particles of different sizes, the particle size distribution in the present case is narrow as most of the particles in the samples are almost of the same size. The particle sizes range between 5–12 μm for 3LMFP and 4–8 μm for 5LMFP; the average particle size estimated from SEM are 8 and 6 μm, respectively. The presence of the pores on the surface of the particles is also revealed in the SEMs taken at the higher magnification [Fig. 2(b, d)]. From the BET surface area measurement data it is confirmed that 5LMFP has larger surface area, pore size and pore volume than 3LMFP (Table 1). The pore size of all samples is concentrated around 40 Å, but pore size distribution (80–200 Å) is better in 5LMFP than in 3LMFP (Fig. 3) because larger pores can be easily filled by electrolyte to enhance Li^+ diffusion. Thus, it follows that the pore size, surface area and particle morphology are dependent on the synthetic conditions.

TEM analysis reveals a nanometer-sized coating of amorphous carbon surrounding the particles, where the LMFP crystallites appear as dark regions and carbon coating appears as gray shade in TEMs (Fig. 4). The thickness of carbon coating in the present case is not as uniform as we have reported for $LiFePO_4$ synthesized by mechanical activation [20–22]. Though a nano-web of carbon of desirable thickness is observed in both the samples, the coating is not uniform as its thickness varies from 9 to 12 nm in 3LMFP [Fig. 4(a)] and 2 to 10 nm in 5LMFP [Fig. 4(b)]. The comparatively thinner coating of porous carbon enveloping 5LMFP particles results in a larger specific surface area, and the higher diffusion of Li^+ with enhanced charge-transfer kinetics and reversible capacity of the cell is expected in this case as compared to 3LMFP. From the region 1200–1700 cm^{-1} in the Raman microprobe spectra, the nature of the residual carbon present in the carbon coating in both LMFP composites can be assessed as a calculated integrated Raman intensity ratio of D/G bands of 2.504 and 1.635 has been observed, respectively, for 3LMFP and 5LMFP (Fig. 5). D/G ratio is an indication of the amount of graphene as compared to the disordered carbon structure, and hence the lower D/G ratio is a measure of higher amount of graphene and also higher electronic conductivity [23]. In the present study, 5LMFP is expected to show better electrochemical properties due to larger amount of graphene in the residual carbon.

Fig. 6 presents the CV behavior of cathodes made of LMFPs. The single redox peak pair for Fe^{3+}/Fe^{2+} redox couple exhibits an anodic oxidation potential at 3.55 V versus Li/Li^+ and a cathodic reduction potential at 3.4 V versus Li/Li^+ for 3LMFP, and at 3.6 and 3.4 V for 5LMFP, respectively. The cathodes showed a respective separation of 150 mV for 3LMFP and 250 mV for 5LMFP between the anodic and cathodic peaks. The oxidation and reduction processes for Mn^{3+}/Mn^{2+} occur at 4.13, 3.89 V for 3LMFP and 4.14, 3.87 V for 5LMFP with a respective peak separation of 0.24 and 0.27 V. The reason for higher separation of potential in 5LMFP is attributed to the penetration of higher electrolyte in its more intense pore structure. When the electrolyte penetrates in these porous particles, resistance is developed. Since the surface area of 5LMFP is higher than that of 3LMFP in this case, there is more resistance in the case of 5LMFP as compared to 3LMFP [10]. These samples exhibit almost similar CV behavior with a small difference in the redox current to be 0.0549 and 0.0578 mA for 3LMFP, as compared to 0.0592 and 0.0719 mA for 5LMFP, corresponding to Mn and Fe. The higher redox current of 5LMFP is indicative of the efficient charge-transfer kinetics of this material that results from its large surface area and thin carbon coating. There is no appreciable change in the redox peak position with cycling, as is apparent from the comparison of CV during the first, second and fifth cycles of the cell prepared with 3LMFP and 5LMFP cathodes (Fig. 6). A slight decrease in current is observed between the first and second cycles; however, on further cycling, it remains nearly the same. Hence, a high reversibility of

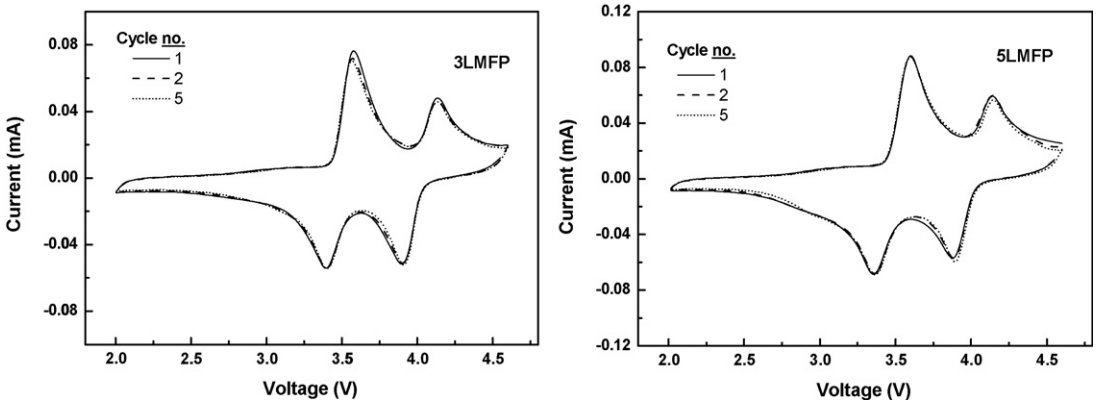

Fig. 6. CV curves during cycling of 3LMFP and 5LMFP (scan rate: 0.1 mV s^{-1}, voltage range: 2.0–4.6 V).

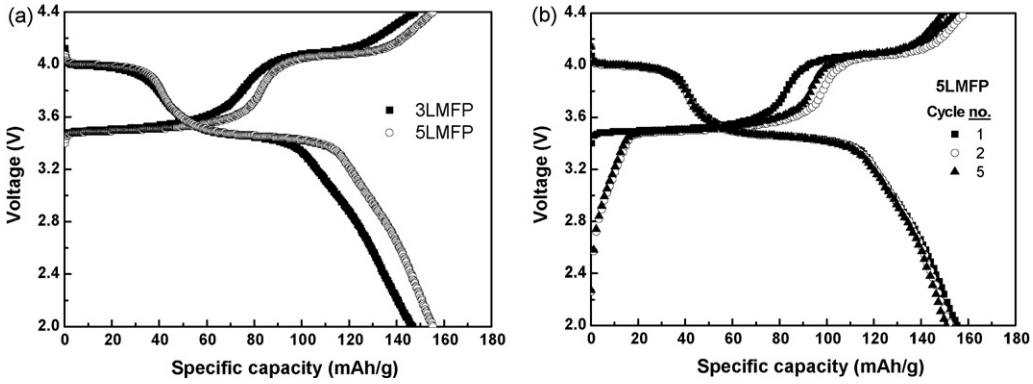

Fig. 7. (a) Initial charge–discharge curves of lithium cells at 0.1 C-rate with cathodes, 3LMFP and 5LMFP and (b) charge–discharge curves of 5LMFP with cycling.

the redox reaction with a stable performance is attained on cycling from both the Li/LMFP cells.

When evaluated as cathode materials in lithium batteries for charge/discharge performance at room temperature, typical flat curves at 4.09 and 3.5 V for Mn^{3+}/Mn^{2+} and Fe^{3+}/Fe^{2+}, respectively, during charge process and 3.99 and 3.45 V for Mn^{3+}/Mn^{2+} and Fe^{3+}/Fe^{2+}, respectively, during discharge process are obtained for 3LMFP; 4.07 and 3.49 V for Mn^{3+}/Mn^{2+} and Fe^{3+}/Fe^{2+}, respectively, during charge process and 4.0 and 3.45 V for Mn^{3+}/Mn^{2+} and Fe^{3+}/Fe^{2+}, respectively, during discharge process for 5LMFP. The voltage separations (ΔV) are 0.1 V for Mn^{3+}/Mn^{2+} and 0.05 V for Fe^{3+}/Fe^{2+} for 3LMFP, and 0.07 V for Mn^{3+}/Mn^{2+} and 0.04 V for Fe^{3+}/Fe^{2+} for 5LMFP as shown in Fig. 7. This means that the cell resistance of the latter is lower, and it also performs as better material than the former as is evident from higher discharge capacities, when tested under same current density. The initial charge and discharge capacities at 0.1 C (0.05 mA cm^{-2}) are, respectively, 148 and 147 mAh g^{-1} for 3LMFP, and 155 and 155 mAh g^{-1} for 5LMFP. The latter shows higher active material utilization (91.2%) during discharge. The charge–discharge performance of the lithium cell prepared with 5LMFP cathode when tested at 0.1 C-rate is shown in Fig. 7(b). The cell reaction voltages at ~3.4 and 4.0 V are in agreement with the observations made from the CV as shown in Fig. 6. The extremely flat cell reaction voltages that are characteristics of $LiFePO_4$ and $LiMnPO_4$ are also observed. The difference between the charging and discharging voltages is very low at 0.1 C (0.04 and 0.07 V). It indicates efficient redox reaction kinetics at a low discharge current. The performance during the first cycle is also retained during subsequent cycles.

Both materials show stable cycle performance upon repeated cycling, when evaluated up to 50 cycles (Fig. 8). The cycle property comparison also shows a better retention of the initial property by 5LMFP than that by 3LMFP. After 50 cycles, 5LMFP retains 97% of the initial discharge capacity at 0.1 C-rate and the value for 3LMFP is 96%. Both 3LMFP and 5LMFP show instability during 6 and 9 cycles, respectively. The reason is considered to be slow penetration of electrolyte and formation of cracks in the carbon layer [10,24]. The electrochemical property evaluation thus shows good performance for both composites prepared by the sol–gel process. The results are extremely encouraging since the LMFP electrode with carbon content of 10 wt.% could perform satisfactorily even at the 0.1 C-rate at 25 °C.

Porous P(VdF-HFP) membrane used as host to prepare gel polymer electrolyte was prepared by electrospinning. The membrane fibers have an average diameter ~1.5 μm whose interlaying generates a microporous structure and it has a porosity of 58% (Fig. 9) [15]. The membrane when soaked in 1 M $LiPF_6$ in EC/DMC sorbed 60 μl of the electrolyte within a few minutes and showed the ionic conductivity of 4.7×10^{-3} S cm^{-1}. The room-temperature charge–discharge behavior of Li/PE/LMFP cell during the first cycle at 0.1 C-rate is shown in Fig. 10(a). The flat voltage plateau for charge and discharge processes occurring in the cell is characteristic of LMFP. The difference in the charge–discharge voltages of Mn and Fe is very low (~0.07 and 0.05 V) indicating the absence of appreciable polarization within the cell at 0.1 C-rate. The charge and discharge capacities are the same 146 mAh g^{-1}, which show high coulombic efficiency of the redox process. The initial discharge capacity of the cell

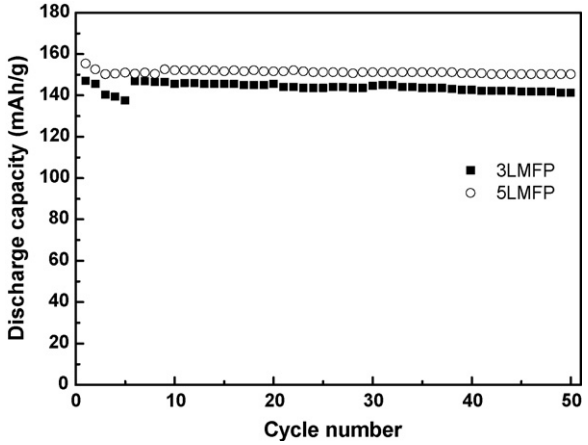

Fig. 8. Cycle performance of lithium cells with LMFP of different heating condition (25 °C, 0.1 C-rate, 2.0–4.6 V).

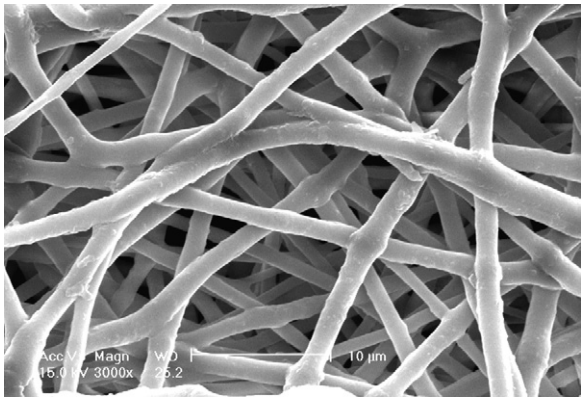

Fig. 9. SEM image of electrospun P(VdF-HFP) membrane.

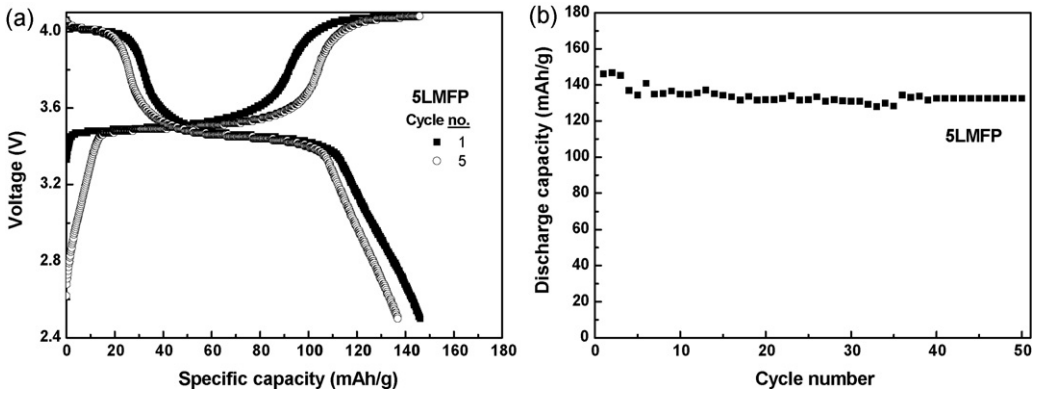

Fig. 10. (a) First and fifth cycle charge–discharge capacities and (b) cycle performance of Li/5LMFP cell with polymer electrolyte based on electrospun P(VdF-HFP) membranes (25 °C, 0.1 C-rate, 2.5–4.2 V).

corresponds to 86% of the theoretical capacity of LMFP. The cell using liquid electrolyte results in a discharge capacity of 155 mAh g^{-1} (91.2% of theoretical capacity). However, the performance of the cell using polymer electrolyte is comparable to that using liquid electrolyte, considering that the cut-off voltages of discharge are 2.0 V for liquid electrolyte and 2.5 V for polymer electrolyte.

The cycle performance of Li/PE/5LMFP cell at room temperature under 0.1 C-rate is shown in Fig. 10(b). In spite of the fact that the discharge capacity decreases with the cycling during 6 cycles, Li/PE/5LMFP cell exhibits a stable cycle property, when studied here up to 50 cycles. Thus, % discharge capacity fade for Li/PE/5LMFP cell calculated on the basis of the initial and 50th cycle capacities is ∼26% per cycle. The remarkably good cycle property of the cell in the present study confirms the excellent efficiency of microporous membrane-based PE to conduct the ions between electrodes without any decrease in the cycling property. This in turn indicates that the polymer electrolyte has good compatibility with both the electrodes.

4. Conclusions

The physical, morphological and electrochemical properties of carbon-coated LMFP synthesized by sol–gel processes with two-step thermal treatments, respectively, at 300 and 700 °C (3LMFP) and at 500 and 700 °C (5LMFP) have been compared. Micron-sized porous particles of active material with high specific surface area along with porous, nano-meter thick web of carbon are obtained. The variation of synthetic conditions impacts the particle size, surface area, and the nature of carbon coating. The performance of room-temperature Li/LMFP cell has been evaluated using liquid electrolyte and polymer electrolyte based on an electrospun P(VdF-HFP) membrane. The cell using polymer electrolyte exhibits initial discharge capacity of 146 mAh g^{-1} (86% of the theoretical capacity of LMFP). The cell using liquid electrolyte results in a discharge capacity of 155 mAh g^{-1} (91.2% of theoretical capacity). The cells including liquid or polymer electrolyte show high initial discharge capacities with high utilization of the active material. The polymer electrolyte exhibits good compatibility as the cell having it exhibits very stable cycle property at 0.1 C-rate with a low capacity fade per cycle (∼0.26%).

Acknowledgements

This research was supported by the Ministry of Knowledge Economy, Korea, under the Information Technology Research Center (ITRC) support program supervised by the Institute of Information Technology Assessment (IITA). Ghanshyam S. Chauhan gratefully acknowledges the Brain Pool Fellowship.

References

[1] A. Yamada, Y. Kudo, K.Y. Liu, J. Electrochem. Soc. 148 (2001) A1153.
[2] A. Yamada, S.C. Chung, J. Electrochem. Soc. 148 (2001) A960.
[3] G. Li, H. Azuma, M. Tohda, Electrochem. Solid-State Lett. 5 (2002) A135.
[4] C. Delacourt, L. Laffont, R. Bouchet, C. Wurm, J.-B. Leriche, M. Morcrette, J.-M. Tarascon, C. Masquelier, J. Electrochem. Soc. 152 (2005) A913.
[5] T. Nakamura, K. Sakumoto, S. Seki, Y. Kobayashi, M. Tabuchi, Y. Yamada, J. Electrochem. Soc. 154 (2007) A1118.
[6] A. Yamada, Y. Takei, H. Koizumi, N. Sonoyama, R. Kanno, K. Itoh, M. Yonemura, T. Kamiyama, Chem. Mater. 18 (2006) 804.
[7] Y. Hu, M.M. Doeff, R. Kostecki, R. Finones, J. Electrochem. Soc. 151 (2002) A1279.
[8] Y.-H. Rho, L.F. Nazar, L. Perry, D. Ryan, J. Electrochem. Soc. 154 (2007) A283.
[9] M. Gaberscek, R. Dominko, M. Bele, M. Remskar, D. Hanzel, J. Jamnik, Solid State Ionics 176 (2005) 1801.
[10] R. Dominko, M. Bele, M. Gaberscek, M. Remskar, D. Hanzel, J.M. Goupil, S. Pejovnik, J. Jamnik, J. Power Sources 153 (2006) 274.
[11] J.K. Kim, G. Cheruvally, J.H. Ahn, J. Solid State Electrochem. 12 (2008) 799.
[12] T. Nakamura, Y. Miwa, M. Tabuchi, Y. Yamada, J. Electrochem. Soc. 15 (2006) A1108.
[13] T.H. Cho, T. Sakai, S. Tanase, K. Kimura, Y. Kondo, T. Tarao, M. Tanaki, Electrochem. Solid-State Lett. 10 (2007) A159.
[14] J.R. Kim, S.W. Choi, S.M. Jo, W.S. Lee, B.C. Kim, J. Electrochem. Soc. 152 (2005) A295.
[15] X. Li, G. Cheruvally, J.K. Kim, J.W. Choi, J.H. Ahn, K.W. Kim, H.J. Ahn, J. Power Sources 167 (2007) 491.
[16] G. Cheruvally, J.K. Kim, J.W. Choi, J.H. Ahn, Y.J. Shin, J. Manuel, P. Raghavan, K.W. Kim, H.J. Ahn, D.S. Choi, C.E. Song, J. Power Sources 172 (2007) 863.
[17] J.K. Kim, G. Cheruvally, X. Li, J.H. Ahn, K.W. Kim, H.J. Ahn, J. Power Sources 178 (2008) 815.
[18] K. Zaghib, K. Striebel, A. Guerfi, J. Shim, M. Armand, M. Gauthier, Electrochim. Acta 50 (2004) 263.
[19] F.S. Fiory, F. Croce, A. D'Epifanio, S. Licoccia, B. Scrosati, E. Traversa, J. Eur. Ceram. Soc. 24 (2004) 1385.
[20] J.K. Kim, J.W. Choi, G. Cheruvally, J.U. Kim, J.H. Ahn, G.B. Cho, K.W. Kim, H.J. Ahn, Mater. Lett. 61 (2007) 3822.
[21] J.K. Kim, G. Cheruvally, J.H. Ahn, H.J. Ahn, J. Phys. Chem. Solids 69 (2008) 1257.
[22] J.K. Kim, G. Cheruvally, J.H. Ahn, G.C. Hwang, J.B. Choi, J. Phys. Chem. 69 (2008) 2371.
[23] M.M. Doeff, Y. Hu, F. McLarnon, R. Kostecki, Electrochem. Solid-State Lett. 6 (2003) A207.
[24] R. Dominko, M. Bele, M. Gaberscek, M. Remskar, D. Hanzel, S. Pejovnik, J. Jamnik, J. Electrochem. Soc. 152 (2005) A607.